2025 26th International Carpathian Control Conference (ICCC) | 979-8-3315-0127-3/25/$31.00 ©2025 IEEE | DOI: 10.1109/ICCC65605.2025.11022852

Control Allocation and Controller Tuning for an Over-Actuated Hexacopter Tilt-Rotor Applied for Precision Agriculture

1st Leandro Oliveira Libório
Department of Electroelectronics
CEFET-MG
Leopoldina, Brasil
leandroliborio94@gmail.com

2nd Gabriel Oliveira Pimentel
Department of Electroelectronics
CEFET-MG
Leopoldina, Brasil
gabriel.pimentel@aluno.cefetmg.br

3rd Murillo Ferreira dos Santos
Department of Electroelectronics
CEFET-MG
Leopoldina, Brasil
murillo.ferreira@cefetmg.br

4th Fernanda Mara Fernandes
Faculty of Minas Gerais
FAMINAS
Muriaé, Brazil
fernandauss@hotmail.com

5th José Lima
Research Centre in Digitalization
and Intelligent Robotics (CeDRI), IPB
Bragança, Portugal
jllima@ipb.pt

6th Maurício Herche Fófano de Morais
Department of Electroelectronics
CEFET-MG
Leopoldina, Brazil
mauricio.fofano@gmail.com

7th Paolo Mercorelli
Institute for Production Technology
and Systems (IPTS), Leuphana University
of Lüneburg, Germany
paolo.mercorelli@leuphana.de

8th Ana Isabel Pereira
Research Centre in Digitalization
and Intelligent Robotics (CeDRI), IPB
Bragança, Portugal
apereira@ipb.pt

***Abstract*—This work presents the control allocation and tuning methodology for an over-actuated Hexacopter Tilt-Rotor (HTR) designed for precision agriculture applications. The HTR's innovative design includes two independently tiltable rotors, enhancing stability and forward velocity, making it suitable for low-altitude maneuvers in agricultural environments. The study focuses on the implementation of a cascade Proportional (P)-Proportional, Integral and Derivative (PID) control structure with Successive Loop Closure (SLC) and the application of an extended Fast Control Allocation (FCA) method to optimize actuator performance. The control gains were meticulously tuned to ensure stability and robustness across six degrees of freedom, achieving precise trajectory tracking and efficient resource use. Validation was conducted through simulations using Robot Operating System (ROS) and Gazebo, replicating realistic precision agriculture scenarios. Results demonstrate the efficacy of the proposed control strategies, highlighting their potential for real-world applications in crop monitoring, pest detection, and resource optimization. Future work includes physical implementation and integration with collaborative robotics.**

***Index Terms*—Unmanned Aerial Vehicle, Hexacopter Tilt-Rotor, UAV Controller, Fast Control Allocation**

The authors are also grateful to CeDRI (UID/05757), SusTEC (LA/P/0007/2021), SmartProduce project, funding by COMPETE2030-FEDER-01204700. They also thank the National Council for Scientific and Technological Development – CNPq, related to project 442696/2023-0.

I. Introduction

Described by their ability to operate without onboard human presence, Unmanned Aerial Vehicles (UAVs) are a current expanding technology. This expansion is attributed to the advances in computational technologies, especially in aerial reconnaissance and terrestrial mapping [1].

Throughout their history, most of the UAV applications have been primarily driven by military purposes, particularly in three main fields: intelligence, surveillance, and reconnaissance [2]. Designed to operate in dangerous environments, these systems were initially developed to perform tasks requiring high precision and maneuverability, such as geographic mapping, communication intercept, and unmanned inspections [3].

Consequently, their versatility and efficiency have facilitated the expansion of UAVs into diverse civilian areas, such as infrastructure inspection (e.g. power lines [4] and construction sites [5]), environmental management (e.g., wildfire control [6]), education [7], traffic monitoring [8], rescue operations [9], health services [10], and agriculture [11].

In the agricultural field, one promising area is Precision Agriculture (PA), which is a strategic approach that uses data on time, location, and individual crop characteristics, processing and analyzing this information alongside other relevant factors to support decision-making. It aims to optimize resource use efficiency, productivity, quality, profitability, and

sustainability in agricultural production to improve productivity and reduce waste [12]. Using UAVs equipped with a variety of sensors, cameras, and the ability to inspect large areas quickly, they can perform a variety of tasks, including weed mapping and control [13], vegetation growth monitoring [14], vegetation health monitoring [15] and disease detection [16].

Moreover, UAVs have revolutionized the PA field due to their ability to perform different maneuvers and fly at low elevations. Being a stable aircraft in these conditions makes them suitable for remote sensing and capturing images with high sharpness and resolution, making data processing more assertive. Considering these aspects and choosing the best UAV for application, it is necessary to consider mass, size, battery, payload capacity, flight autonomy, acquisition cost, and weather conditions, among others [17].

UAVs are classified into three primary categories: fixed-wing, rotary-wing, and hybrid-wing systems. Fixed-wing UAVs (e.g., airplanes) are characterized by their ability to carry larger payloads over longer distances. Rotary-wing UAVs (e.g., helicopters and multicopters) are more versatile, with variations in weight and the number of rotors. Hybrid-wing UAVs (e.g., tiltrotors and balloons) combine the advantages of rotary-wing and fixed-wing systems, allowing vertical take-off and landing while also achieving efficient and high-speed horizontal flight, making them a promising solution for complex operational scenarios [18].

Given this promising field, some works were explored and can be highlighted. The study [19] described using a hexacopter RGB, multispectral, and thermal images for weed mapping in a corn field using multisource remote sensing data. The research highlights that thermal measurements significantly improve weed mapping accuracy. The results showed that this fusion of data outperforms traditional models in weed detection, and the use of the UAV plays a crucial role in collecting high-resolution data, ensuring efficient monitoring.

Moreover, as discussed in [20], many UAVs are operated manually to monitor crops and capture images. For PA, environmental pollution caused by pesticides and agrochemicals is a critical factor. Professional pilot's operation of UAV may present human error and be expensive. To improve this spraying practice, the focus is on the project efficiency of the basic manipulators to perform a necessary agricultural activity and the path planning, navigation, and guidance algorithms adapted to the desired scenarios. Studies on computational fluid dynamics and numerical simulation of the spray drift movement using UAV aim to mitigate problems of indirect contamination to the environment. Furthermore, the development of path planning, navigation, and guidance algorithms adapted to different scenarios of open fields, greenhouses, sheds, etc., eliminates the probability of human error. These techniques improve production, economic and resource efficiency, and environmental impact.

In this context, this study focuses on developing and controlling an over-actuated HTR UAV prototype. Equipped with six motors, two independently adjusted by servomotors, this aircraft achieves excellent stability and faster flight, making it ideal for PA applications. Simulated environments were created using ROS and Gazebo software to evaluate its performance. A cascade multilevel topology P-PID controller, implemented with SLC, was applied. The experimental results confirmed the UAV's effectiveness.

Moreover, this study continues the research previously introduced in [21] and substantially collaborates in international cooperation, aiming to create an advanced cooperative system that integrates robots and autonomous agents for field inspection.

Although previous work focused on the overall design of the cooperative system, this study offers a more detailed analysis of the control tuning process. It provides a deeper insight into the configuration and performance of the control loops. Furthermore, this research expands on the validation of the system, testing it in a different scenario that demonstrates its practical application and efficiency under varied conditions.

The key scientific contributions of this study include:

- Development and implementation of an HTR in a simulated virtual environment;
- Simulations of the HTR in PA scenarios within ROS and Gazebo software;
- Apply the extended FCA method, considering totally coupled Control Effectiveness Matrixs (CEMs).

The remaining sections of this work are organized as described below: Section II shows the kinematic and dynamics modeling of the HTR, Section III describes the control architecture designed for the proposed aircraft, and the control allocation algorithm apply, Section IV shows the experimental results obtained with flight simulations. Then, Section V concludes the work presented here.

II. UAV Kinematic and Dynamic Modeling

This section aims to present the modeling process, including both the kinematic and dynamic definitions and concepts, which outlines the mathematical model of the over-actuated HTR. Subsequently, Fig. 1 presents a detailed view of the aircraft:

Fig. 1. Illustration of the proposed HTR.

In this configuration, the two tiltrotors are positioned horizontally by maintaining a 90-degree pitch angle, which consid-

erably increases the forward and backward velocity of the HTR without requiring changes to its pitch angle. This configuration allows for a more energy-efficient flight by minimizing energy consumption, as the HTR reduces drag force.

The HTR's variables are measured relative to three reference frames: $\mathcal{F}^v$, which represents the vehicle frame; $\mathcal{F}^b$, which represents the fixed body frame, along with the inertial frame $\mathcal{F}^i$. In addition, the aircraft has six Degrees of Freedom (DoFs): translational movements along the x, y, and z axes, and angular dynamics described by roll (ϕ), pitch (θ), and yaw (ψ).

The HTR kinematic and dynamic behavior of a hexacopter can be described according to the following state variables: the vector $\boldsymbol{\eta_1} = [p_n, p_e, h]^T$ represents the north, east and altitude position along axis $\hat{\boldsymbol{i}}^i, \hat{\boldsymbol{j}}^i$ and -$\hat{\boldsymbol{k}}^i$, respectively, in the inertial frame ($\mathcal{F}^i$); the vector $\boldsymbol{\eta_2} = [\phi, \theta, \psi]^T$ represents roll, pitch, and yaw angles defined concerning vehicle frame ($\mathcal{F}^v$). The vectors $\boldsymbol{v_1} = [u, v, w]^T$ and $\boldsymbol{v_1} = [p, q, r]^T$ represent the three-dimensional linear and angular velocities along the axis $\hat{\boldsymbol{i}}^b$, $\hat{\boldsymbol{j}}^b$ and $\hat{\boldsymbol{k}}^b$, respectively, in the fixed body frame ($\mathcal{F}^b$).

In general, the aircraft's position is expressed by the vector $\boldsymbol{\eta_1} \in \mathbb{R}^3$ within the inertial frame $\mathcal{F}^i$, and its orientation is given by $\boldsymbol{\eta_2} \in \mathbb{R}^3$ in the vehicle frame $\mathcal{F}^v$. Additionally, the linear and the angular velocities denoted as $\boldsymbol{v_1} \in \mathbb{R}^3$ and $\boldsymbol{v_2} \in \mathbb{R}^3$, are measured within the frame $\mathcal{F}^b$. According to the study [22], (3) establishes the default nomenclature:

$$\boldsymbol{\eta_1} = [p_n, p_e, h]^T, \tag{1}$$
$$\boldsymbol{\eta_2} = [\phi, \theta, \psi]^T, \tag{2}$$
$$\boldsymbol{\eta} = [\boldsymbol{\eta_1}, \boldsymbol{\eta_2}]^T, \tag{3}$$

with velocities:

$$\boldsymbol{v_1} = [u, v, w]^T, \tag{4}$$
$$\boldsymbol{v_2} = [p, q, r]^T, \tag{5}$$
$$\boldsymbol{v} = [\boldsymbol{v_1}, \boldsymbol{v_2}]^T, \tag{6}$$

where $\boldsymbol{v} \in \mathbb{R}^6$ represents the velocity vector, with $\boldsymbol{v_1} \in \mathbb{R}^3$ denoting the linear velocity vector and $\boldsymbol{v_2} \in \mathbb{R}^3$ representing the angular velocity vector, both expressed in the fixed body frame $\mathcal{F}^b$.

Moreover, the aircraft's full model describing the kinematics and dynamics is summarized in (7):

$$\dot{\boldsymbol{\eta}} = \boldsymbol{J}\boldsymbol{v}, \tag{7}$$

where $\boldsymbol{\eta} \in \mathbb{R}^6$ is the velocity vector in the inertial frame $\mathcal{F}^i$, and $\boldsymbol{J} \in \mathbb{R}^6$ is the Jacobian matrix, expressed as follows [23]:

$$\boldsymbol{J} \triangleq \begin{pmatrix} J_x & -J_{xy} & -J_{xz} \\ -J_{xy} & J_y & -J_{yz} \\ -J_{xz} & -J_{yz} & J_z \end{pmatrix}. \tag{8}$$

Therefore, the HTR exhibits symmetry along the coordinate axes, leading to the moments of inertia satisfying $J_{xz} = J_{xy} = J_{yz} = 0$.

In this context, the HTR dynamics model is represented by differential equations derived using the Newton–Euler method, such as shown [22]:

$$\boldsymbol{I^b}\dot{\boldsymbol{v}} + \boldsymbol{C^b}(\boldsymbol{v})\boldsymbol{v} - \boldsymbol{\tau_a^b} - \boldsymbol{\tau_g^b} = \boldsymbol{\tau_p^b}, \tag{9}$$

where $\boldsymbol{I^b} \in \mathbb{R}^{6\times6}$ is the system inertia matrix, $\boldsymbol{C^b}(\boldsymbol{v}) \in \mathbb{R}^{6\times6}$ is the Coriolis–centripetal matrix in the frame $\mathcal{F}^b$, $\boldsymbol{\tau_a^b}, \boldsymbol{\tau_g^b}, \boldsymbol{\tau_p^b} \in \mathbb{R}^6$ are the resultant vectors for Aerodynamics, Gravitational, and Propulsion forces, respectively.

Because the UAV does not have support surfaces, the aerodynamic torques can be disregarded, as the HTR's Center of Gravity (CG) aligns with the aerodynamic center.

III. Controller Topology and Tuning

This section focuses on the implemented control structure, including the control loops developed for the HTR within the specific control gains used. Following this, it is introduced the control allocation algorithm used, an extension of the FCA technique.

UAVs are controlled by a flight system consisting of two main components: external and internal loops. The external one generates position and altitude references, while the internal loop (also implemented onboard) processes these references to velocities [24]. Among the various control strategies commonly utilized, P and PID controllers are widely recognized for their effectiveness. The PID control is the most common control approach used due to its value and intuition in practical implementations.

In this context, this presented work employs a sophisticated control structure, not only in the control allocation task: the cascade P-PID topology. This configuration features two cascade levels: an external level employing a P controller and an internal level using a PID controller. The output from the external controller acts as the input for the internal cascade controller, enhancing the dynamic response to ensure precision and robustness in control. The overall schematic representation of the HTR control structure is depicted in Fig. 2:

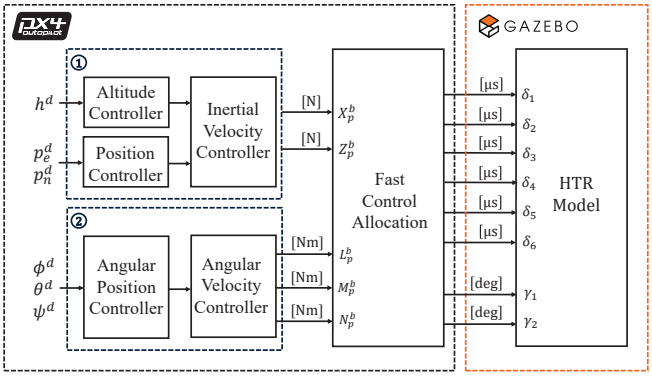

Fig. 2. Illustration of overall HTR control structure.

The control loops shown in Figs. 3 and 4 represents the P-PID control of the HTR's state variables, which are linked to position, velocity, and orientation. Each state variable is

controlled by a PID that has the gains K_p, K_d, and K_i, acting on the difference between the desired and fundamental error. The block FCA is the control allocation task extended in this work. The "Kinematics and Dynamics of HTR" block represents the UAV mathematical modeling.

In this context, the control tuning process was performed using the aircraft linear model, based on the works [25] and [23]. Table I presents the P-PID controller gains that were adopted with a fine-tuning:

TABLE I
CONTROLLER GAINS UTILIZED IN THE SIMULATION.

Variable	P		
p_n	$k_p^n = 0.960$		
p_e	$k_p^e = 0.942$		
h	$k_p^h = 2.050$		
ϕ	$k_p^\phi = 5.600$		
θ	$k_p^\theta = 6.450$		
ψ	$k_p^\psi = 5.300$		
	P	**I**	**D**
u	$k_p^u = 3.050$	$k_i^u = 0.460$	$k_d^u = 0.105$
v	$k_p^v = 3.020$	$k_i^v = 0.450$	$k_d^v = 0.098$
w	$k_p^w = 4.100$	$k_i^w = 2.050$	$k_d^w = 0.110$
p	$k_p^p = 0.140$	$k_i^p = 0.185$	$k_d^p = 0.0025$
q	$k_p^q = 0.145$	$k_i^q = 0.195$	$k_d^q = 0.0035$
r	$k_p^r = 0.185$	$k_i^r = 0.190$	$k_d^r = 0.0032$

A. Extended Fast Control Allocation Algorithm

A major challenge in implementing nonlinear control strategies for unmanned systems is the significant computational cost. This issue becomes even more critical for compact, lightweight devices requiring real-time processing. The FCA method addresses this challenge by simplifying the nonlinear control allocation problem into a computationally efficient linear process through two distinct steps: separation and mapping [23].

This technique is built on a faster linear variant than the traditional approach outlined in [23]. This technique (FCA) divides the Real Control Action (RCA) into groups, separating the complex nonlinear problem into simpler linear subproblems. Mapping is then applied to associate each Virtual Control Action (VCA) with its corresponding linear subproblem. Initially, the nonlinear system is described by:

$$\hat{\boldsymbol{\tau}} = \boldsymbol{M}(\boldsymbol{u}), \tag{10}$$

where $\boldsymbol{M}$ is the UAV's CEM, and $\hat{\boldsymbol{\tau}}$ and u represent the VCA and RCA vectors, respectively.

This method creates new linear spaces derived from the nonlinear one, enabling the problem to be split into two distinct subproblems [23]:

$$\begin{aligned} \hat{\boldsymbol{\tau}}_{\boldsymbol{a}} &= \boldsymbol{M_a}(\boldsymbol{u_b})\boldsymbol{u'_a}, && (11)\\ &= X_p^b, && (12)\\ \hat{\boldsymbol{\tau}}_{\boldsymbol{b}} &= \boldsymbol{M_b}(\boldsymbol{u_a})\boldsymbol{u_b}, && (13)\\ &= (X_p^b, Z_p^b, L_p^b, M_p^b, N_p^b)^T. && (14) \end{aligned}$$

where $\boldsymbol{u_a} \in \mathbb{R}^q$ is the a subset of the system's n actuators, with $q \in \mathbb{N}^*$, and $\boldsymbol{u_b} \in \mathbb{R}^r$ denotes the remaining actuators, with $r \in \mathbb{N}^*$. The terms $\hat{\boldsymbol{\tau}}_{\boldsymbol{a}} \in \mathbb{R}^{ma}$ and $\hat{\boldsymbol{\tau}}_{\boldsymbol{b}} \in \mathbb{R}^{mb}$ represent the contributions to RCA, where $m \in \mathbb{N}^*$ is the number of DoFs. In addition, $\boldsymbol{M_a}(\boldsymbol{u_a}) \in \mathbb{R}^{ma \times q}$ and $\boldsymbol{M_b}(\boldsymbol{u_b}) \in \mathbb{R}^{mb \times r}$ define the corresponding mapping matrices.

The term X_p^b was chosen for the first VCA subgroup because it is driven by $\boldsymbol{u_a}$. In other words, the servomotors (γ_i) are driven by the VCA X_p^b. The others VCA variables are assigned to $\boldsymbol{u_b}$ (propulsion motors δ_i), as shown below:

$$\begin{aligned} \boldsymbol{u'_a} &= [s\gamma_1, s\gamma_2, 1]^T, && (15)\\ \boldsymbol{u_a} &= [s^-\gamma_1, s^-\gamma_2]^T, && (16)\\ \boldsymbol{u_b} &= [\delta_1, \delta_2, \delta_3, \delta_4, \delta_5, \delta_6]^T. && (17) \end{aligned}$$

Additionally, $\boldsymbol{M_a}(\boldsymbol{u_a}) \in \mathbb{R}^{1\times 6}$ and $\boldsymbol{M_b}(\boldsymbol{u_b}) \in \mathbb{R}^{5\times 6}$ are denoted by (18) and (19), respectively:

IV. EXPERIMENTAL RESULTS

The experiments were derived from simulations of the vehicle using ROS and Gazebo software, which offers a flexible virtual environment for testing. The simulations focused on a real-world PA application.

The location of the simulated flight was selected on an open field at the Polytechnic Institute of Bragança due to its safe and controlled environment to validate the use of the HTR in a PA scenario where accurate navigation over crops is essential. Fig. 5 provides an aerial view:

Fig. 5. flight path planned in the PA scenario.

The controlled variables of altitude, linear velocity, and attitude angles were analyzed to assess the aircraft's performance. Fig. 6(a) presents the five controlled responses.

The results indicate that the aircraft successfully achieved the intended altitude profile, stabilizing at the target level. This demonstrates its ability to maintain precise navigation throughout the designated area.

Regarding the attitude variables, the roll angles remained closely aligned with the SetPoint (SP). As expected, the pitch remained near zero, given that the tiltrotors are responsible for managing this control aspect. Meanwhile, yaw exhibited more variations due to nose adjustments required for trajectory tracking, confirming the system's effectiveness.

Fig. 6(b) illustrates the RCA responses of the HTR along the flight. The propulsion motors behaved as anticipated, following the simulated trajectory. The expected variations occurred

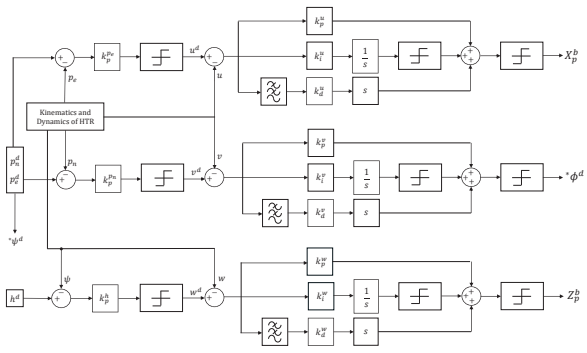

Fig. 3. HTR's high level structure.

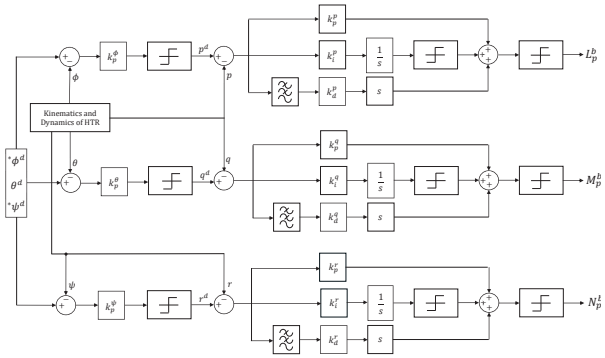

Fig. 4. HTR's low level control structure.

$$X_p^b = \begin{pmatrix} k_1\delta_1 & k_1\delta_2 & 0 \end{pmatrix} \begin{pmatrix} s\gamma_1 \\ s\gamma_2 \\ 1 \end{pmatrix}, \tag{18}$$

$$\begin{pmatrix} X_p^b \\ Z_p^b \\ L_p^b \\ M_p^b \\ N_p^b \end{pmatrix} = \begin{pmatrix} k_1 s\gamma_1 & k_1 s\gamma_2 & 0 & 0 & 0 & 0 \\ k_1 c\gamma_1 & k_1 c\gamma_2 & k_1 & k_1 & k_1 & k_1 \\ k_1 c\gamma_1 l - k_2 s\gamma_1 & -k_1 c\gamma_2 l + k_2 s\gamma_2 & k_1 l\frac{1}{2} & -k_1 l\frac{1}{2} & -k_1 l\frac{1}{2} & k_1 l\frac{1}{2} \\ 0 & 0 & k_1 l\frac{\sqrt{3}}{2} & -k_1 l\frac{\sqrt{3}}{2} & k_1 l\frac{\sqrt{3}}{2} & -k_1 l\frac{\sqrt{3}}{2} \\ -k_1 s\gamma_1 l - k_2 c\gamma_1 & +k_1 s\gamma_2 l + k_2 c\gamma_2 & -k_2 & k_2 & k_2 & -k_2 \end{pmatrix} \begin{pmatrix} \delta_1 \\ \delta_2 \\ \delta_3 \\ \delta_4 \\ \delta_5 \\ \delta_6 \end{pmatrix}. \tag{19}$$

mainly during turns and tiltrotor adjustments. Additionally, when motors 1 and 2 tilted, a temporary reduction in total lift was observed, requiring compensation from the remaining RCA. Consequently, the other motors increased their thrust to counterbalance the lift loss.

Moreover, during straight-line segments, the tiltrotors maintained a positive angle to ensure the HTR sustained a zero-pitch position for stable forward motion.

V. Conclusions

This paper was divided into four main stages: Kinematic and dynamic modeling of the proposed HTR; Implementation of the HTR in a simulated virtual environment in Gazebo; Implementation and tuning of the control loops; Experimental simulations for validations.

Based on the results of this work, a stable and functional HTR effectively followed the proposed trajectories, proving to be a promising innovative approach for areas such as PA. With the growing demand for automated solutions and collaborative robots for complex tasks, the HTR offers a highly adaptable platform. The modular architecture of the aircraft allows the integration of computer vision techniques, enabling detailed crop monitoring, disease detection, and highly efficient harvest optimization.

Alternative control allocation techniques and investigating the aircraft's performance with a more varied set of subsystems can be studied for future work.

Acknowledgment

The authors thank CEFET-MG and Leuphana Universität Lüneburg for their support.

References

[1] F. P. Leme, "Sistema embarcado para controle de plataforma de dois eixos utilizada em veiculos aereos nao tripulados," *UNICAMP*, 2017.

[2] P. G. Fahlstrom, T. J. Gleason, and M. H. Sadraey, *Introduction to UAV systems*. John Wiley & Sons, 2022.

[3] M. N. Tahir, Y. Lan, Y. Zhang, H. Wenjiang, Y. Wang, and S. M. Z. A. Naqvi, "Application of unmanned aerial vehicles in precision agriculture," in *Precision Agriculture*, pp. 55–70, Elsevier, 2023.

[4] V. M. Leal Lopes, L. M. Honório, M. F. Santos, A. A. Pancoti, M. F. Silva, L. F. Diniz, and P. Mercorelli, "Design of an over-actuated hexacopter tilt-rotor for landing and coupling in power transmission lines," *Drones*, vol. 7, no. 6, p. 341, 2023.

[5] H. Noh, S. Kwon, Y. S. Park, and S.-B. Woo, "Application of rgb uav imagery to sea surface suspended sediment concentration monitoring in coastal construction site," *Applied Ocean Research*, vol. 145, p. 103940, 2024.

[6] D. Perikleous, G. Koustas, S. Velanas, K. Margariti, P. Velanas, and D. Gonzalez-Aguilera, "A novel drone design based on a reconfigurable unmanned aerial vehicle for wildfire management," *Drones*, vol. 8, no. 5, p. 203, 2024.

[7] M. M. Bolick, E. A. Mikhailova, and C. J. Post, "Teaching innovation in stem education using an unmanned aerial vehicle (uav)," *Education Sciences*, vol. 12, no. 3, p. 224, 2022.

[8] B. Cherif, H. Ghazzai, and A. Alsharoa, "Lidar from the sky: Uav integration and fusion techniques for advanced traffic monitoring," *IEEE Systems Journal*, 2024.

[9] D. Han, H. Jiang, L. Wang, X. Zhu, Y. Chen, and Q. Yu, "Collaborative task allocation and optimization solution for unmanned aerial vehicles in search and rescue," *Drones*, vol. 8, no. 4, p. 138, 2024.

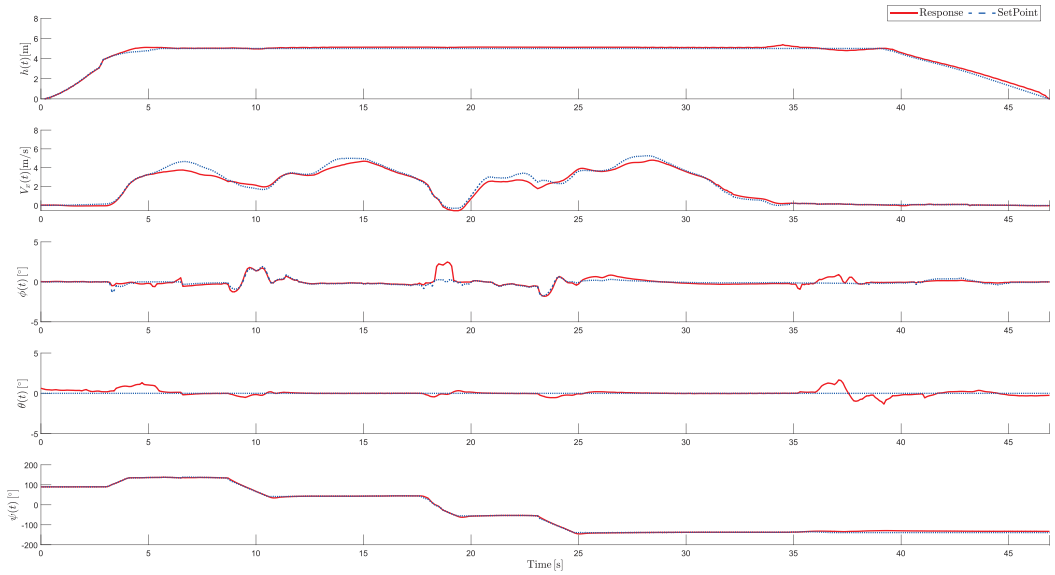

(a) Altitude (h), linear velocity (V_x), roll (ϕ), pitch (θ) and yaw (ψ) controlled responses.

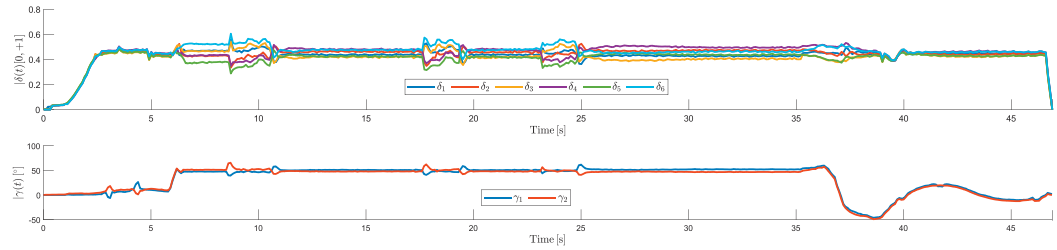

(b) HTR (δ_i) and servomotors tilting angles (γ_i).

Fig. 6. HTR controlled responses.

[10] M. A. Ghaffar, L. Peng, M. U. Aslam, M. Adeel, and S. Dassari, "Vehicle-uav integrated routing optimization problem for emergency delivery of medical supplies," *Electronics*, vol. 13, no. 18, p. 3650, 2024.

[11] A. Aeberli, S. Phinn, K. Johansen, A. Robson, and D. W. Lamb, "Characterisation of banana plant growth using high-spatiotemporal-resolution multispectral uav imagery," *Remote Sensing*, vol. 15, no. 3, p. 679, 2023.

[12] S. K. Phang, T. H. A. Chiang, A. Happonen, and M. M. L. Chang, "From satellite to uav-based remote sensing: A review on precision agriculture," *IEEE Access*, vol. 11, pp. 127057–127076, 2023.

[13] M. Gašparović, M. Zrinjski, D. Barković, and D. Radočaj, "An automatic method for weed mapping in oat fields based on uav imagery," *Computers and electronics in agriculture*, vol. 173, p. 105385, 2020.

[14] Y. Cao, G. L. Li, Y. K. Luo, Q. Pan, and S. Y. Zhang, "Monitoring of sugar beet growth indicators using wide-dynamic-range vegetation index (wdrvi) derived from uav multispectral images," *Computers and Electronics in Agriculture*, vol. 171, p. 105331, 2020.

[15] J. Guerra-Hernández, R. A. Díaz-Varela, J. G. Ávarez-González, and P. M. Rodríguez-González, "Assessing a novel modelling approach with high resolution uav imagery for monitoring health status in priority riparian forests," *Forest Ecosystems*, vol. 8, p. 61, 2021.

[16] A. I. de Castro, J. M. Peña, J. Torres-Sánchez, F. M. Jiménez-Brenes, F. Valencia-Gredilla, J. Recasens, and F. López-Granados, "Mapping cynodon dactylon infesting cover crops with an automatic decision tree-obia procedure and uav imagery for precision viticulture," *Remote sensing*, vol. 12, no. 1, p. 56, 2019.

[17] M. R. B. Júnior, B. R. de Almeida Moreira, V. dos Santos Carreira, A. L. de Brito Filho, C. Trentin, F. L. P. de Souza, D. Tedesco, T. Setiyono, J. P. Flores, Y. Ampatzidis, *et al.*, "Precision agriculture in the united states: A comprehensive meta-review inspiring further research, innovation, and adoption," *Computers and Electronics in Agriculture*, vol. 221, p. 108993, 2024.

[18] J. Agrawal and M. Y. Arafat, "Transforming farming: A review of ai-powered uav technologies in precision agriculture," *Drones*, vol. 8, no. 11, p. 664, 2024.

[19] B. Xu, R. Meng, G. Chen, L. Liang, Z. Lv, L. Zhou, R. Sun, F. Zhao, and W. Yang, "Improved weed mapping in corn fields by combining uav-based spectral, textural, structural, and thermal measurements," *Pest Management Science*, vol. 79, no. 7, pp. 2591–2602, 2023.

[20] K. Lochan, A. Khan, I. Elsayed, B. Suthar, L. Seneviratne, and I. Hussain, "Advancements in precision spraying of agricultural robots: A comprehensive review," *IEEE Access*, 2024.

[21] G. O. Pimentel, M. F. d. Santos, J. Lima, P. Mercorelli, and F. M. Fernandes, "An over-actuated hexacopter tilt-rotor uav prototype for agriculture of precision: Modeling and control," *Sensors*, vol. 25, no. 2, 2025.

[22] M. F. Santos, L. M. Honório, A. P. G. M. Moreira, M. F. Silva, and V. F. Vidal, "Fast real-time control allocation applied to over-actuated quadrotor tilt-rotor," *Journal of Intelligent & Robotic Systems*, 2021.

[23] M. Santos, L. Honório, A. P. G. M. Moreira, P. A. N. Garcia, M. Silva, and V. F. Vidal, "Analysis of a fast control allocation approach for nonlinear over-actuated systems," *ISA transactions*, vol. 126, pp. 545–561, 2022.

[24] F. Toscano, C. Fiorentino, N. Capece, U. Erra, D. Travascia, A. Scopa, M. Drosos, and P. D'Antonio, "Unmanned aerial vehicle for precision agriculture: A review," *IEEE Access*, 2024.

[25] R. Beard and T. McLain, *Small Unmanned Aircraft: Theory and Practice*. Princeton University Press, 2012.